1). These two effects cancel each other, resulting in little net change in community-level variance.

For species-level variances, the effect of interspecific competition depends on the mean intrinsic rates of increase, r_i, as predicted by the analytical results (Fig. 2). It also depends on the correlation in species responses to environmental fluctuations, ρ. As ρ increases, species biomasses tend to vary in synchrony, causing the magnitudes of intra- and interspecific competition to vary in concert. This reduces the contrast between the effects of intra- and interspecific competition on species-level variances (Fig. 2, A versus B and C versus D).

Increasing the number of species n in most cases decreases community-level variances (Fig. 3). To understand why, we consider two communities with n and $n + 1$ species having the same total biomass and no interspecific competition. When $\rho = 0$, species biomasses are not correlated, and the variance in total biomass equals the sum of variances in species biomasses. Variances in total biomass for the two communities are related by $V^c_{n+1} = [n/(n + 1)]V^c_n$. This reduction in community-level variance with increasing n has been called "statistical averaging" (*10*) or the "portfolio effect" (*11*). When species respond similarly to environmental fluctuations ($\rho > 0$), $V^c_{n+1} = [n/(n + 1)]\{(1 + n\rho_s)/[1 + (n - 1)\rho_s]\}V^c_n$, where ρ_s is the correlation between species biomasses. Thus, when ρ, and consequently ρ_s, approaches 1, V^c_{n+1} approaches V^c_n, resulting in no effect of species number on community-level variances. Finally, species number has the same effect in communities with interspecific competition, because the amplification of community-level variances is independent of whether competition is intra- or interspecific (Fig. 2). Thus, increasing n decreases community-level variances by introducing species that respond differently to environmental fluctuations.

Our main result is that interspecific competition and species number have little influence on community-level variances; the variance in total community biomass depends only on how species respond to environmental fluctuations. This contrasts with arguments (*3, 12*) that interspecific competition may decrease community-level variances by driving negative covariances between species abundances. We show that negative covariances are counteracted by increased species-level variances created by interspecific competition.

Consequently, assessing the effect of biodiversity on community variability should emphasize species-environment interactions and differences in species' sensitivities to environmental fluctuations (for example, drought-tolerant species and phosphorus-limited species) (*5, 13*). Competitive interactions are relatively unimportant except through their effects on mean abundances. We have focused on competitive communities, because much current experimental work has addressed competition among plants. Nonetheless, the same results can be shown to hold for more complex models with multiple trophic levels.

References and Notes

1. R. H. MacArthur, *Ecology* **36**, 533 (1955); C. S. Elton, *The Ecology of Invasions by Plants and Animals* (Chapman & Hall, London, 1958); R. Margalef, *Brookhaven Symp. Biol.* **22**, 25 (1969); S. L. Pimm, *Nature* **307**, 321 (1984).
2. R. M. May, *Nature* **238**, 413 (1972); *Stability and Complexity in Model Ecosystems* (Princeton Univ. Press, Princeton, NJ, ed. 2, 1974).
3. D. Tilman and J. A. Downing, *Nature* **367**, 363 (1994); D. Tilman, *Ecology* **77**, 350 (1996).
4. S. L. Pimm, *The Balance of Nature?* (Chicago Univ. Press, Chicago, 1991).
5. S. J. McNaughton, *Am. Nat.* **111**, 515 (1977).
6. A. R. Ives, *Ecol. Monogr.* **65**, 217 (1995); A. R. Ives and V. A. A. Jansen, *Ecology* **79**, 1039 (1998).
7. V_k and U_k are the variances of the projections of $\mathbf{X}(t)$ and $\mathbf{E}(t)$, respectively, onto vector w_k.
8. This follows immediately from the community matrix with diagonal elements $1 - [r/(\alpha + 1)]$ and off-diagonal elements $-r\alpha/[(n - 1)(\alpha + 1)]$.
9. Model A is

$$x_i(t+1) = x_i(t)\exp\left\{\varepsilon_i(t) + r_i\left[1 - \frac{x_i(t) + \frac{\alpha}{n-1}\sum_{j\neq i}^{n} x_j(t)}{K_i}\right]\right\}$$

The competition coefficient α is scaled by $1/(n - 1)$ so that the net strength of interspecific competition is independent of the number of species. Model B is

$$x_i(t+1) = x_i(t)\exp\left\{\varepsilon_i(t) + r_i\left[1 - \frac{x_i(t)}{K_i/(1+\alpha)}\right]\right\}$$

K_i is decremented by $1/(1 + \alpha)$ to produce the same reduction in biomass as model A. For both models, $\varepsilon_i(t)$ values are selected from a multivariate normal distribution with mean 0, variance 0.1, correlation ρ, and no serial correlation.
10. D. F. Doak *et al.*, *Am. Nat.* **151**, 264 (1998).
11. D. Tilman, C. L. Lehman, C. E. Bristow, *ibid.*, p. 277; D. Tilman, *Ecology* **80**, 1455 (1999).
12. J. H. Lawton and V. K. Brown, in *Biodiversity and Ecosystem Function*, E. D. Schulze and H. A. Mooney, Eds. (Springer-Verlag, Berlin, 1993), pp. 255–270; T. M. Frost, S. R. Carpenter, A. R. Ives, T. K. Kratz, in *Linking Species and Ecosystems*, C. G. Jones and J. H. Lawton, Eds. (Chapman & Hall, New York, 1994), pp. 224–239.
13. S. J. McNaughton, *Ecol. Monogr.* **55**, 259 (1985).

14. We thank D. F. Doak, T. M. Frost, S. L. Pimm, N. Schellhorn, D. Tilman, M. G. Turner, and especially S. R. Carpenter for comments and insights. Supported by a grant from NSF.

12 July 1999; accepted 7 September 1999

CFTR Chloride Channel Regulation by an Interdomain Interaction

Anjaparavanda P. Naren,[1]* Estelle Cormet-Boyaka,[1]* Jian Fu,[1] Matteo Villain,[1] J. Edwin Blalock,[1] Michael W. Quick,[1,2] Kevin L. Kirk[1,2]†

The cystic fibrosis gene encodes a chloride channel, CFTR (cystic fibrosis transmembrane conductance regulator), that regulates salt and water transport across epithelial tissues. Phosphorylation of the cytoplasmic regulatory (R) domain by protein kinase A activates CFTR by an unknown mechanism. The amino-terminal cytoplasmic tail of CFTR was found to control protein kinase A–dependent channel gating through a physical interaction with the R domain. This regulatory activity mapped to a cluster of acidic residues in the NH_2-terminal tail; mutating these residues proportionately inhibited R domain binding and CFTR channel function. CFTR activity appears to be governed by an interdomain interaction involving the amino-terminal tail, which is a potential target for physiologic and pharmacologic modulators of this ion channel.

The CFTR chloride channel is implicated in two major human diseases: cystic fibrosis, a genetic disorder that is caused by reduced CFTR function in the lung (*1*), and secretory diarrhea, a fluid and electrolyte disorder that is caused by increased CFTR activity in the gut (*2*). The development of strategies for treating either of these diseases would be facilitated by detailed knowledge of how to activate or inactivate the CFTR channel. The opening and closing of the CFTR channel (gating) is regulated by hydrolysis of adenosine triphosphate (ATP) by one or both of the nucleotide binding domains (NBDs; Fig. 1A)

[1]Department of Physiology and Biophysics, [2]Department of Neurobiology, Gregory Fleming James Cystic Fibrosis Research Center, University of Alabama at Birmingham, Birmingham, AL 35294, USA.

*These authors contributed equally to this report.
†To whom correspondence should be addressed. E-mail: kirk@phybio.bhs.uab.edu

within the channel (*3–5*). However, the initial step in activating CFTR is phosphorylation of the R domain by protein kinase A (PKA), which relieves an inhibitory effect of this domain on ATP-dependent gating through a poorly understood mechanism (*6–8*). Whether the phosphorylated R domain interacts with other CFTR domains to stabilize the activated state of the channel is unknown.

We addressed the role of the NH_2-terminal tail of CFTR (N-Tail) in the gating process. The N-Tail physically links CFTR to protein components of the membrane traffic machinery (*9–11*), and one of these proteins inhibits steady-state CFTR currents through direct binding to the N-Tail (*9, 10*). These observations suggested to us the possibility that the N-Tail has a previously unrecognized role in CFTR channel regulation.

In a mutational analysis of the N-Tail, we identified a cluster of acidic residues that regulate steady-state CFTR activity (Fig. 1). We centered our analysis on a highly charged region of the N-Tail that is well conserved across species: residues 46 to 60 (Fig. 1B). [A naturally occurring mutation at one of these positions (Asp^{58}) associates with mild disease (*12*)]. We replaced each of the charged residues within this region with alanine. A subset of the mutants exhibited lower adenosine 3′,5′-monophosphate (cAMP)–activated macroscopic currents than that of wild-type channels when expressed in *Xenopus* oocytes (Fig. 1C) (*13*). None of these alanine substitutions at charged positions affected biosynthesis of CFTR, with the exception of Glu^{60} → Ala, which inhibited processing of the channel in the endoplasmic reticulum and was not characterized further (*14*). Some, but not all, of the substitutions at acidic positions inhibited CFTR currents, whereas the basic residues within this region appeared to contribute little to CFTR activity (Fig. 1C). The relative

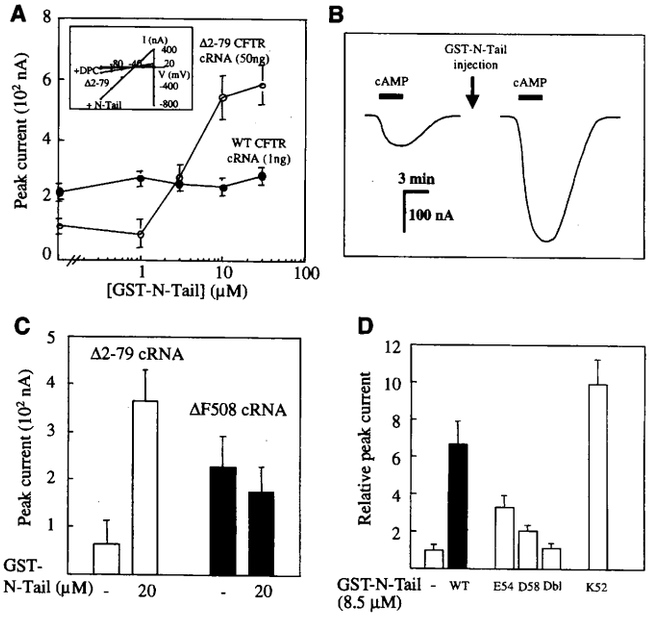

Fig. 2. Stimulation of the activity of the N-Tail deletion mutant Δ2-79 CFTR by recombinant N-Tail peptide. **(A)** cRNAs for Δ2-79 CFTR or wild-type CFTR were injected into oocytes 5 days before voltage clamp analysis. More Δ2-79 CFTR cRNA was injected (50 ng versus 1 ng for wild-type CFTR) because this deletion mutant is a biosynthetic processing mutant (*9, 10*). N-Tail peptide also had no effect on wild-type CFTR currents at higher cRNA amounts [10 ng (*19*)]. GST fusion protein containing residues 1 to 75 (GST–N-Tail) was microinjected to varying final concentrations (estimated assuming an oocyte volume of 1 μl) 15 to 30 min before activating currents with 200 μM dibutyrl cAMP, 20 μM forskolin, and 5 mM IBMX. Shown are peak cyclic AMP-induced increases in current at −50 mV holding potential (n = 4 to 9 oocytes for each data point). Inset: Current-voltage traces for cAMP-activated Δ2-79 CFTR currents in the absence of GST–N-Tail, in the presence of GST–N-Tail (3 μM), and in the presence of GST–N-Tail plus 0.5 mM DPC. **(B)** Δ2-79 CFTR currents for an individual oocyte before and 15 min after injection of 3 μM GST–N-Tail. Currents were activated with cAMP (black bars) at −50 mV as described above. **(C)** Failure of GST–N-Tail to stimulate the transport activity of the ΔF508 CFTR processing mutant. Amount of cRNA, 50 ng (n = 5 to 6 oocytes for each data point). **(D)** Effects of mutant N-Tail fusion proteins on cAMP-activated Δ2-79 CFTR currents (n = 4 to 8 oocytes for each data point). Peak cAMP-activated current is expressed relative to that in the absence of peptide.

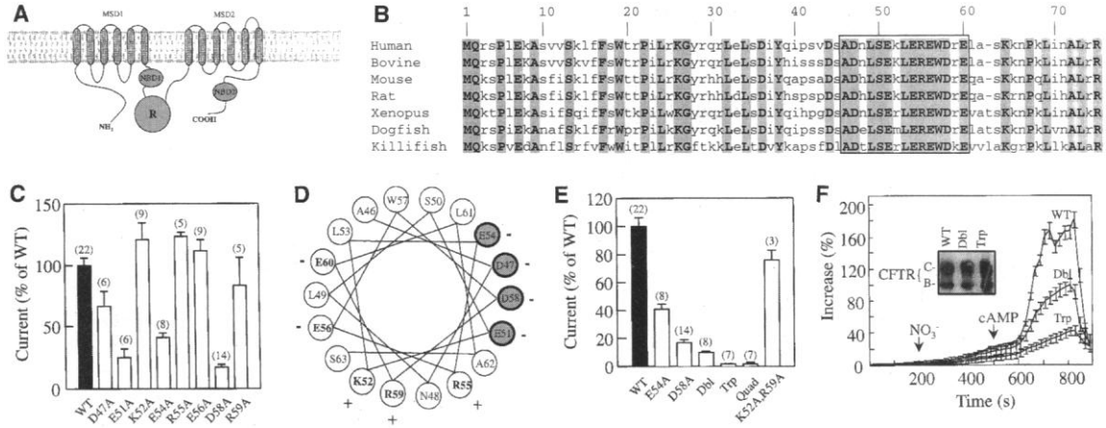

Fig. 1. Regulation of CFTR activity by a cluster of acidic residues in the NH_2-terminal tail. **(A)** Schematic of CFTR. MSD, membrane-spanning domain. **(B)** Sequence alignments of the NH_2-terminal tails of the indicated species. Strictly conserved residues are shaded. Residues 46 to 60 are enclosed in a box. **(C)** Peak cAMP-activated currents mediated by the indicated CFTR N-Tail mutants expressed in *Xenopus* oocytes. Equivalent amounts of cRNA (2 ng) were injected into oocytes 2 to 4 days before two-electrode voltage clamp analysis (*9, 10*). Macroscopic currents were activated with 100 μM dibutyryl cAMP, 1 mM 3-isobutyl-1-methylxanthine (IBMX), and 20 μM forskolin, and were recorded at −50 mV holding potential. The currents for each mutant construct are expressed as a percentage of that for wild-type channels assayed in the same batch of oocytes on the same day. Numbers of oocytes are shown in parentheses. **(D)** Helical wheel plot of residues 46 to 63. Functionally important acidic residues are in bold circles. **(E)** Graded loss of CFTR current activity by successive elimination of negative charge in the N-Tail (double: E54A, D58A; triple: D47A, E54A, D58A; quadruple: D47A, E51A, E54A, D58A). **(F)** Lower halide transport of N-Tail mutants in COS-7 cells. Inset: Mature protein (band C) and immature protein (band B) after electrophoresis. COS-7 cells were transfected as described (*9, 10*). Transport activity was assayed as the increase in fluorescence of an intracellular dye that is quenched by halides [6-methoxy-*N*-(3-sulfopropyl) quinolinium (*11*)]. Extracellular I^- was replaced with NO_3^- at the time indicated by the first arrow. A cAMP activating mixture (10 μM forskolin, 100 μM 8-(4-chlorophenylthio)-cAMP, 100 μM IBMX) was added (second arrow) (n = 94 to 146 cells for each data point). Error bars denote SEM. CFTR immunoprecipitations were done on parallel samples as described (*9, 10*). Abbreviations for the amino acid residues are as follows: A, Ala; C, Cys; D, Asp; E, Glu; F, Phe; G, Gly; H, His; I, Ile; K, Lys; L, Leu; M, Met; N, Asn; P, Pro; Q, Gln; R, Arg; S, Ser; T, Thr; V, Val; W, Trp; and Y, Tyr.

position of the acidic residues within the linear sequence of the N-Tail was not the critical determinant of functional importance (for example, the $Glu^{56} \rightarrow$ Ala mutant functioned normally, whereas substitutions at Glu^{54} and Asp^{58} caused inhibition of the maximal current in the presence of cAMP). Residues 46 to 63 in the N-Tail are predicted to form an α helix on the basis of secondary structure features and circular dichroism spectral analysis (*15*). The acidic residues that appear to be most critical for CFTR current activity partition onto one surface of this putative helix (Fig. 1D). The successive elimination of negative charge in this region led to a graded inhibition of cAMP-dependent currents in oocytes (Fig. 1E) (*16*). These N-Tail mutants also exhibited lower activity when expressed in COS-7 fibroblasts and assayed with a standard fluorometric assay of halide transport (Fig. 1F), even though equivalent amounts of mature wild-type or mutant protein were produced. Thus, the sequential removal of negative charge in this region of the N-Tail led to a graded inhibition of CFTR function.

The results of the mutational analysis imply that the N-Tail is a positive regulator of CFTR activity, and that certain acidic residues in the tail are essential for this regulatory activity. To verify that the N-Tail has a positive regulatory activity, we determined whether the currents mediated by an N-Tail deletion mutant (Δ2-79 CFTR) could be stimulated by microinjecting recombinant N-Tail peptide into oocytes expressing Δ2-79 CFTR (Fig. 2). This N-Tail deletion mutant (and all other NH_2-terminal deletion constructs that we have analyzed) generates very low cAMP-activated currents in oocytes, in part because these deletion mutants are inefficiently processed in the biosynthetic pathway (*10, 11*). However, Δ2-79 CFTR is also inhibited because of the loss of a positive regulatory activity exerted by the N-Tail. Microinjection of a glutathione-S-transferase (GST) fusion protein containing the N-Tail (GST–N-Tail) increased the cAMP-dependent currents mediated by Δ2-79 CFTR in a dose-dependent fashion (Fig. 2A). These currents were determined to be CFTR-mediated on the basis of their approximately linear current-voltage behavior (Fig. 2A), their sensitivity to the chloride channel blocker diphenylamine carboxylate (DPC), and their single-channel properties in cell-attached patches (*17*). The stimulation of Δ2-79 CFTR–mediated currents by GST–N-Tail occurred within 15 to 30 min of microinjecting the peptide (representative traces, Fig. 2B) and therefore was not due to an effect on Δ2-79 CFTR synthesis. The N-Tail peptide had no effect on the currents mediated by wild-type CFTR (Fig. 2A) or by another CFTR construct that already has the NH_2-terminal tail, ΔF508 CFTR [a biosynthetic processing mutant that is the most common CF mutant (Fig. 2C) (*18*)]. Moreover, this stimulatory effect of GST–N-Tail could be inhibited in a graded fashion by mutating one or both of the acidic residues at positions 54 and 58 in this peptide (Fig. 2D), but not by mutating either of the basic residues at positions 52 (Fig. 2D) and 59 (*19*). Taken together, our results indicate that the N-Tail is a positive regulator of CFTR function, and that a cluster of acidic residues in the tail is essential for this regulatory activity.

The isolated N-Tail may physically interact with another region of the molecule to stimulate CFTR activity. To test for such a biochemical interaction, we monitored the binding of GST–N-Tail fusion protein to the intact CFTR molecule. Wild-type CFTR from COS-7 cell extracts associated with, and could be precipitated by, GST–N-Tail, but not by GST alone (Fig. 3A). However, the efficiency of binding to N-Tail was reduced for a CFTR deletion construct (ΔR-S660A) that lacked a portion of the R domain (amino acids 708 to 835; Fig. 3A, right panel). Recombinant R domain (amino acids 595 to 855) expressed in COS-7 cells also formed a complex with the GST–N-Tail peptide in a solution binding assay (Fig. 3B). The isolated R domain did not bind to GST alone or to the other CFTR fusion proteins that we have tested [cytoplasmic loops 1, 2, or 3 (*20*)]. Binding between the intact R domain and N-Tail was saturable, with a median effective concentration of about 1 μM GST–N-Tail (Fig. 3, E and F).

We also tested a series of R domain fragments for N-Tail binding (Fig. 3, C and D). An NH_2-terminal fragment of the R domain (amino acids 595 to 740) retained binding activity, whereas a COOH-terminal fragment (amino acids 708 to 835) did not bind the N-Tail fusion protein. Similar results were obtained in a direct binding assay with a synthetic biotinylated N-Tail peptide (amino acids 30 to 63) and GST–R domain fusion proteins as binding partners (Fig. 3D). The binding of the biotinylated peptide to the NH_2-terminal R domain fragment was specific in that it could be inhibited by a 100-fold molar excess of unlabeled N-Tail peptide, but not by excess irrelevant control peptide. The fact that the COOH-terminal R domain fragment (amino acids 708 to 835) has little N-Tail binding activity seems paradoxical because the R domain deletion construct (ΔR-S660A) that inefficiently interacts with GST–N-Tail lacks only this region of the R domain (Fig. 3A, right panel). However, in quantitative binding assays the NH_2-terminal fragment of the R domain bound the N-Tail with lower apparent affinity than did the intact R domain (Fig. 3, E and F). Thus, the N-Tail appears to bind to a region within the NH_2-terminal portion of the R domain, but the apparent affinity of this interaction is evidently enhanced by the presence of the COOH-terminal region of this domain.

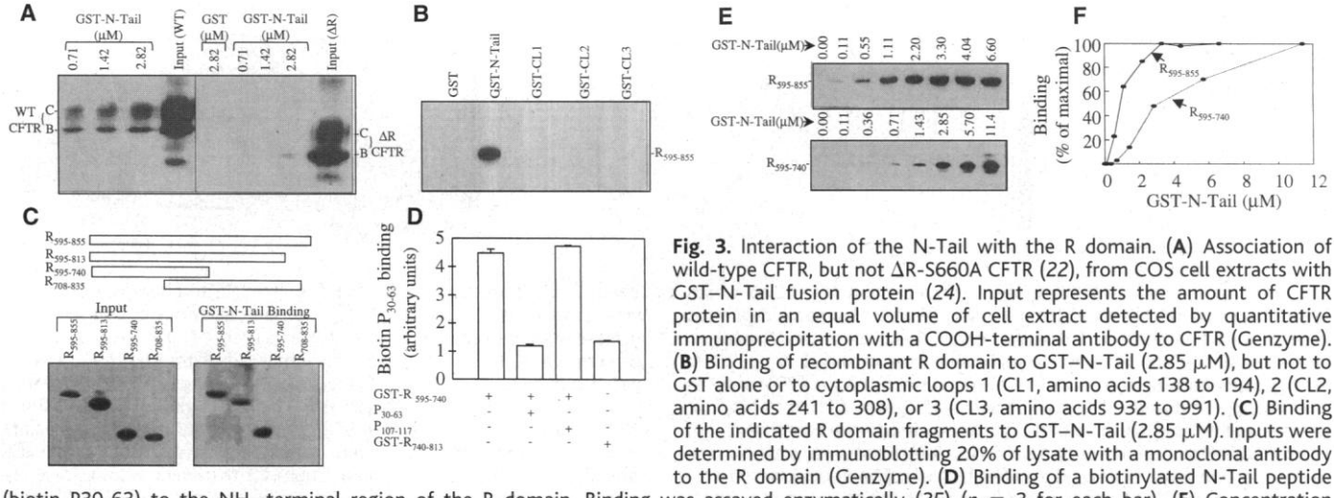

Fig. 3. Interaction of the N-Tail with the R domain. (**A**) Association of wild-type CFTR, but not ΔR-S660A CFTR (*22*), from COS cell extracts with GST–N-Tail fusion protein (*24*). Input represents the amount of CFTR protein in an equal volume of cell extract detected by quantitative immunoprecipitation with a COOH-terminal antibody to CFTR (Genzyme). (**B**) Binding of recombinant R domain to GST–N-Tail (2.85 μM), but not to GST alone or to cytoplasmic loops 1 (CL1, amino acids 138 to 194), 2 (CL2, amino acids 241 to 308), or 3 (CL3, amino acids 932 to 991). (**C**) Binding of the indicated R domain fragments to GST–N-Tail (2.85 μM). Inputs were determined by immunoblotting 20% of lysate with a monoclonal antibody to the R domain (Genzyme). (**D**) Binding of a biotinylated N-Tail peptide (biotin P30-63) to the NH_2-terminal region of the R domain. Binding was assayed enzymatically (*25*) (n = 3 for each bar). (**E**) Concentration dependence of GST–N-Tail binding to intact R domain (amino acids 595 to 855) and NH_2-terminal R domain fragment (amino acids 595 to 740), assayed as in (B). (**F**) Corresponding binding curves; binding is normalized to maximal binding observed for each R domain construct.

The binding of the N-Tail to the R domain was disrupted by the same N-Tail mutations that inhibited CFTR currents (Fig. 4). The N-Tail mutant in which alanine replaced all four acidic residues at critical positions (amino acids 47, 51, 54, and 58) exhibited reduced binding to recombinant R domain, especially at low peptide concentrations (Fig. 4A). This mutant peptide was also less effective at interacting with intact CFTR protein from cell extracts (*21*). The double mutant ($Glu^{54} \rightarrow Ala$, $Asp^{58} \rightarrow Ala$) exhibited R domain binding that was intermediate between that for wild-type N-Tail and the mutant that lacked all four acidic residues, whereas the elimination of the two basic residues at positions 52 and 59 had little effect on binding (Fig. 4B). Recombinant R domain (amino acids 595 to 855) that was expressed in COS-7 cells and phosphorylated in vivo also was competent for N-Tail binding, exhibiting an affinity for the N-Tail that was equal to or slightly greater than that of unphosphorylated R domain (Fig. 4C).

In kinetic studies and patch clamp experiments, we observed that the activated state of the CFTR channel was destabilized by mutations in the N-Tail that disrupt R domain binding (Fig. 5). Relative to wild-type CFTR, the N-Tail mutants exhibited 2 to 4 times the rate of current deactivation in oocytes after removal of a cAMP stimulus (Fig. 5A). In addition, the mutants that lacked three or four of the critical acidic residues in the N-Tail exhibited reduced channel open probabilities and decreased burst durations (open-channel lifetimes) in excised membrane patches under conditions that maximally activate wild-type CFTR (Fig. 5, B and C). To determine whether the effects of these N-Tail mutations on channel gating require an intact R domain, we also eliminated the four critical acidic residues from the ΔR-S660A CFTR construct. This deletion mutant exhibited a small amount of PKA-independent activity (Fig. 5D) (*22, 23*). Introducing the N-Tail mutations had no effect on this constitutive activity in excised membrane patches. Thus, N-Tail mutations that inhibit R domain binding appear to affect CFTR gating in the presence, but not absence, of an intact R domain.

Our results indicate that CFTR chloride channel activity is stabilized by an interaction between the R domain and the NH_2-terminal tail. This interdomain interaction is dependent on a cluster of strictly conserved acidic residues in the N-Tail. CFTR channel gating appears to be tightly controlled by this interaction between the N-Tail and R domain, as evidenced by the graded loss of activity with the successive removal of negative charge in the N-Tail. The N-Tail appears not to modulate CFTR activity by globally influencing phosphorylation of the R domain; we detected no effects of any of the N-Tail mutations on steady-state phosphorylation in vitro or in vivo (*21*). We favor the notion that the N-Tail modulates channel activity by controlling access of the phosphorylated R domain to inhibitory or stimulatory sites within the channel (*22, 23*). The control of CFTR gating by the NH_2-terminal tail implies that the intracellular traffic of CFTR and the gating of this ion channel may be coupled processes, because components of the membrane traffic

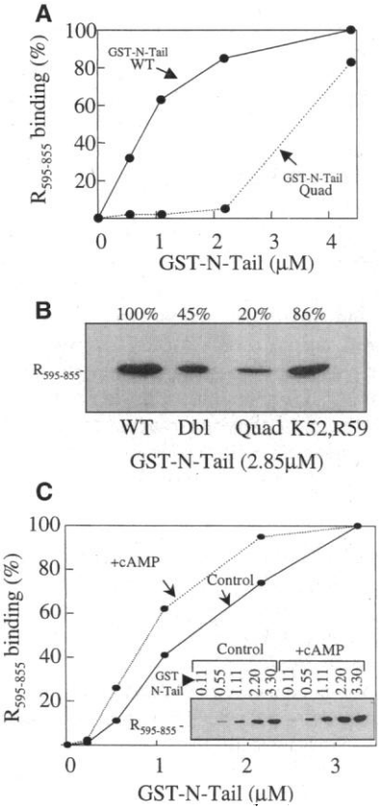

Fig. 4. Effects on the N-Tail R domain interaction of mutating acidic residues in the N-Tail and of phosphorylation of the R domain. (**A**) R domain binding to wild-type N-Tail fusion protein and to fusion protein containing all four mutations (Quad). Assay was as described for Fig. 3F. Binding is normalized to maximal binding observed for wild-type N-Tail fusion protein. (Repeated three times with similar results.) (**B**) Graded decrease in R domain binding exhibited by double mutant (Dbl; E54A, D58A) and by mutant lacking all four acidic residues. Binding to K52A, R59A was unaffected. Percent binding relative to that of wild-type N-Tail fusion protein is shown above each lane. (Repeated four times with similar results.) (**C**) Effect on N-Tail binding of phosphorylating recombinant R domain in vivo. Transfected COS-7 cells were activated with cAMP (see Fig. 1F) for 10 min before cell lysis. Binding is normalized to the maximal binding observed for unphosphorylated R domain. (Repeated three times with the same results.)

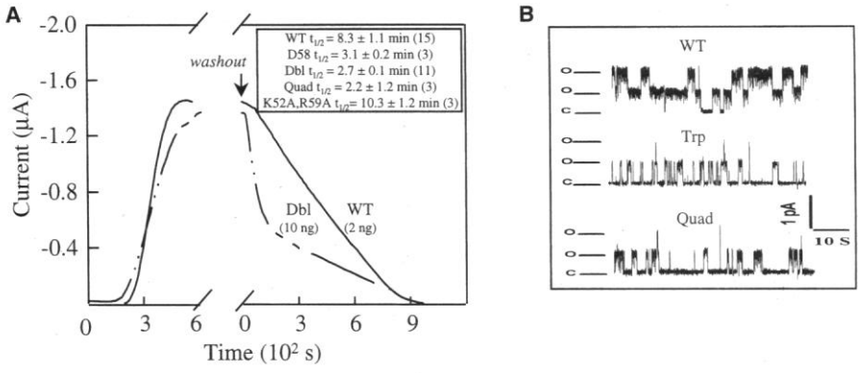

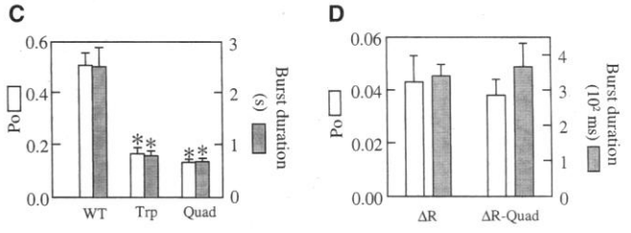

Fig. 5. Destabilization of CFTR channel activity by N-Tail mutations that disrupt R domain binding. (**A**) Activation and deactivation kinetics after addition and washout of 10 μM forskolin and 5 mM IBMX to oocytes expressing the indicated CFTR constructs. Inset shows mean half-times for current deactivation, with numbers of oocytes in parentheses. D58A, double, and quadruple mutant cRNAs were injected in amounts 5 times that of wild-type CFTR. (**B**) Representative single-channel records for wild-type CFTR, triple N-Tail mutant, and quadruple N-Tail mutant in excised membrane patches in the presence of PKA (80 U/ml) and 1.5 mM Mg-ATP. Holding potential was −80 mV. Each patch had two active channels. (**C**) Mean open probabilities and open-channel burst durations estimated as described (*26*). Numbers of patches analyzed were 10 (wild-type), 9 (triple), and 10 (quadruple). Asterisk for each mutant indicates significant difference ($p < 0.01$) from wild-type levels by unpaired t test. (**D**) Estimated open probabilities and open-channel burst durations for ΔR-S660A CFTR ($n = 5$) and for ΔR-S660A with the four N-Tail mutations (Quad; $n = 5$) in the presence of 1.5 mM Mg-ATP but no PKA.

machinery can physically interact with this tail (*9–11*). Proteins that bind to this tail have the potential to modulate CFTR gating by stabilizing or disrupting its interaction with the R domain. The NH_2-terminal tail of CFTR could serve as a target for physiologic regulators of CFTR gating or for pharmacologic maneuvers to modulate CFTR activity.

References and Notes

1. M. J. Welsh and A. E. Smith, *Cell* **73**, 1251 (1993).
2. S. E. Gabriel, K. N. Brigman, B. H. Koller, R. C. Boucher, M. J. Stutts, *Science* **266**, 107 (1994).
3. T. Baukrowitz, T. C. Hwang, A. C. Nairn, D. C. Gadsby, *Neuron* **12**, 473 (1994).
4. M. R. Carson, S. M. Travis, M. J. Welsh, *J. Biol. Chem.* **270**, 1711 (1995).
5. D. J. Wilkinson *et al.*, *J. Gen. Physiol.* **107**, 103 (1996).
6. S. H. Cheng *et al.*, *Cell* **66**, 1066 (1989).
7. C. E. Bear *et al.*, *ibid.* **68**, 809 (1992).
8. C. J. Matthews *et al.*, *J. Physiol. (London)* **508**, 365 (1998).
9. A. P. Naren *et al.*, *Nature* **390**, 302 (1997).
10. A. P. Naren *et al.*, *Proc. Natl. Acad. Sci. U.S.A.* **95**, 10972 (1998).
11. L. S. Prince *et al.*, *J. Biol. Chem.* **274**, 3602 (1999).
12. Cystic Fibrosis Genetic Analysis Consortium (www.genet.sickkids.on.ca/cftr).
13. All point mutations were introduced into a 1-kb fragment of the CFTR coding region by the Quickchange site-directed mutagenesis kit (Stratagene). This fragment was sequenced completely to verify each mutation and then ligated into pCDNA3 vector (Invitrogen) containing the rest of the CFTR coding region.
14. A. P. Naren, E. Cormet-Boyaka, K. L. Kirk, unpublished data.
15. A. P. Naren, M. Villain, D. Muccio, K. L. Kirk, unpublished data.
16. The triple and quadruple N-Tail mutants are not completely inactive; for example, cAMP-activated currents can be detected when higher cRNA amounts for these mutants are injected. Indeed, because of the nonlinearity of the oocyte expression system, the currents mediated by these mutants can approach (but not reach) wild-type levels at very high cRNA amounts (such as 50 ng).
17. J. Fu and K. L. Kirk, unpublished data.
18. S. H. Cheng *et al.*, *Cell* **63**, 827 (1990).
19. M. W. Quick and K. L. Kirk, unpublished data.
20. Recombinant NBD1 (amino acids 433 to 584) bound weakly to GST–N-Tail, but this binding was not inhibited by the N-Tail mutations that inhibit CFTR channel activity.
21. A. P. Naren and K. L. Kirk, unpublished data.
22. M. C. Winter and M. J. Welsh, *Nature* **387**, 294 (1997).
23. J. Ma, J. Zhao, M. L. Drumm, J. Xie, P. B. Davis, *J. Biol. Chem.* **272**, 28133 (1997).
24. Assays were done as described (*9, 10*). Briefly, soluble GST–N-Tail peptide was added to a lysate of COS-7 cells [0.2% Triton X-100 in phosphate-buffered saline (PBS)] transiently expressing recombinant CFTR (or various R domain constructs) and mixed for 1 hour at room temperature. Bound proteins were precipitated with excess glutathione agarose, washed extensively in 0.2% Triton X-100 in PBS, and analyzed for CFTR or R domain by immunoblotting with monoclonal antibodies to the COOH-terminus or R domain (Genzyme). CFTR immunoprecipitations were done on portions of the same lysates (*9, 10*).
25. Peptides were synthesized on a PerSeptive Biosystems 9050 peptide synthesizer. The biotin was conjugated to the NH_2-terminus with fluorenyl methoxycarbonyl-amino caproic acid as spacer. Peptide binding (biotin P30-63) was assessed by mixing 1.25 μM peptide and 2.5 μM soluble GST-R domain peptide in PBS for 1 hour at 22°C. A 100-fold molar excess of unbiotinylated peptide was used for competition experiments. The complex was precipitated with excess glutathione agarose and washed with PBS. Streptavidin–horseradish peroxidase (HRP, 1 μM) was added in PBS and incubated for 20 min. The beads were washed extensively in PBS plus 0.2% Triton X-100 and assayed for HRP activity with 2,2′-azinobis(3-ethylbenzothiozoline)-6 sulfonic acid (ABTS) according to manufacturer's instructions (Pierce, St. Louis, MO).
26. The single-channel properties of wild-type CFTR and the N-Tail mutants were analyzed in inside-out membrane patches excised from oocytes. The pipette solution contained 140 mM *N*-methyl-D-glucamine (NMDG), 0.2 mM $CaCl_2$, 0.5 mM $MgCl_2$, and 10 mM Hepes (pH to 7.4 with HCl). The bath solution contained 140 mM NMDG, 0.5 mM $MgCl_2$, 1 mM EGTA, and 10 mM Hepes (pH to 7.4 with HCl) supplemented with 1.5 mM Mg-ATP and PKA catalytic subunit (80 U/ml, Promega). Records of multichannel patches (holding potential −80 mV) were digitized using an Axopatch 200B amplifier, filtered at 200 Hz, and analyzed using PCLAMP 6.0 software. The open probabilities of the N-Tail mutants should be considered to be maximal estimates given the very brief open times of these mutants, which leads to underestimating channel number. Open-channel burst durations were estimated with the cycle time method and a minimal interburst duration of 20 ms (*8*). The N-Tail mutants also exhibited reduced open-channel burst durations relative to wild-type CFTR when analyzed at shorter minimal interburst durations such as 10 ms; however, this gave an underestimate of the true open-channel burst duration. The single-channel properties of the ΔR CFTR constructs were analyzed in membrane patches excised from transfected HeLa cells as described (*22*) with a minimal interburst duration of 20 ms. All patch clamp experiments were performed at 20° to 22°C.

27. We thank M. Welsh for providing the original ΔR-S660A CFTR construct. Supported by NIH grants DK51868 and DK50830 (K.L.K.), DA10509 (M.W.Q.), and MH52527 (J.E.B.).

1 June 1999; accepted 26 August 1999

Neurogenesis in the Neocortex of Adult Primates

Elizabeth Gould,* Alison J. Reeves, Michael S. A. Graziano, Charles G. Gross

In primates, prefrontal, inferior temporal, and posterior parietal cortex are important for cognitive function. It is shown that in adult macaques, new neurons are added to these three neocortical association areas, but not to a primary sensory area (striate cortex). The new neurons appeared to originate in the subventricular zone and to migrate through the white matter to the neocortex, where they extended axons. These new neurons, which are continually added in adulthood, may play a role in the functions of association neocortex.

The traditional view of the adult primate neocortex is that it is structurally stable and that neurogenesis and synapse formation occur only during development (*1, 2*). Yet structural plasticity in adult brains is found both among lower vertebrates (*3*) and in phylogenetically older mammalian structures such as the olfactory bulb and hippocampus (*4, 5*), even in primates (*6, 7*). Furthermore, neurogenesis is widespread in the adult avian brain including in the hyperstriatum (*8, 9*), a structure homologous to the mammalian cerebral cortex (*10*). Thus, it may seem paradoxical that there is no compelling evidence for neurogenesis in the neocortex of adult mammals (*11*) and there are even strong claims against it for primates (*1*). Using bromodeoxyuridine (BrdU) labeling, which marks proliferating cells and their progeny (*12*), combined with retrograde tract tracing and immunohistochemistry for neuronal markers, we attempted to resolve this paradox. We report that in adult macaques, new neurons are indeed added to several regions of association cortex where they extend axons. The presence of new neurons in brain areas involved in learning and memory (*13*) supports earlier suggestions that adult-generated neurons may play a role in these functions (*9, 14, 15*).

We injected 12 adult *Macaca fascicularis* with BrdU and used immunohistochemistry for cell-specific markers to examine BrdU-labeled cells in prefrontal, inferior temporal, posterior parietal, and striate cortex (*16*). The following markers were used: for mature neurons, (i) NeuN (neuronal nuclei), (ii) NSE (neuron-specific enolase), or (iii) MAP-2 (microtubule-associated protein-2); for immature neurons, TOAD-64 (turned-on-after-division 64-kD protein); for astroglia, GFAP (glial fibrillary acidic protein) (*17, 18*).

In animals perfused 1 week or more after the last BrdU injection, we observed BrdU-labeled cells in prefrontal, inferior temporal, and parietal cortex (Figs. 1 and 2; Table 1). In the region of the principal sulcus in prefrontal cortex, the majority (62% to 84%) of BrdU-labeled cells had round or oval nuclei, morphological characteristics of mature neurons (nuclear diameter = 10 to 25 μm). Confocal laser scanning microscopic analysis of immunostained tissue (*19*) indicated that a subset of these cells expressed markers of mature neurons (Figs. 1 through 3; Table 1). BrdU-

Department of Psychology, Princeton University, Princeton, NJ 08544, USA.

*To whom correspondence should be addressed. E-mail: goulde@princeton.edu

References and Notes

[2] **Cystic Fibrosis Heterozygote Resistance to Cholera Toxin in the Cystic Fibrosis Mouse Model**

Sherif E. Gabriel; Kristen N. Brigman; Beverly H. Koller; Richard C. Boucher; M. Jackson Stutts

Science, New Series, Vol. 266, No. 5182. (Oct. 7, 1994), pp. 107-109.

Stable URL:

http://links.jstor.org/sici?sici=0036-8075%2819941007%293%3A266%3A5182%3C107%3ACFHRTC%3E2.0.CO%3B2-L

[10] **Syntaxin 1A Inhibits CFTR Chloride Channels by means of Domain-Specific Protein-Protein Interactions**

Anjaparavanda P. Naren; Michael W. Quick; James F. Collawn; Deborah J. Nelson; Kevin L. Kirk

Proceedings of the National Academy of Sciences of the United States of America, Vol. 95, No. 18. (Sep. 1, 1998), pp. 10972-10977.

Stable URL:

http://links.jstor.org/sici?sici=0027-8424%2819980901%2995%3A18%3C10972%3AS1ICCC%3E2.0.CO%3B2-K